Microscopic insight into structural and optical properties of glassy TeO2 derived from finite-cluster ab initio modelling

O. Noguera, M.B. Smirnov, E.M. Roginskii, P. Thomas

Version of Record: https://www.sciencedirect.com/science/article/pii/S0921452622009012
Manuscript_27390277fdc72b745fba9bd9909371e6

Microscopic insight into structural and optical properties of glassy TeO_2 derived from finite-cluster ab initio modelling

O Noguera[1*], M B Smirnov[2] E M Roginskii[3] and P Thomas[1]

[1]Institut de Recherche sur les Céramiques (IRCER), UMR CNRS 7315, Université de Limoges, Centre Européen de la Céramique, 12 rue Atlantis, 87068 Limoges, France

[2]St Petersburg State University, Petrodvoretz, 194508 St Petersburg, Russia

[3]Ioffe Institute, Polytekhnicheskaya 26, 194021 St. Petersburg, Russia

[*]corresponding author. Centre Européen de la Céramique, 12 rue Atlantis, 87068 Limoges, France. Phone number: +33(0) 5 87 50 23 89; Fax number: +33(0) 587 50 23 04; E-mail address: olivier.noguera@unilim.fr

Abstract

The paper reports on theoretical analysis of structural and non-linear optical properties of different size and shape TeO_2 clusters using *ab initio* hybrid functional approximation to density functional theory. The obtained structural properties reveal uncommon structural units for crystal, which are common for amorphous tellurium oxide glass. The pair distribution function reproduces the experimental data in very good agreement, as well as the calculated phonon density and the Raman spectra. The finite field method was applied to evaluate the values of third order nonlinear susceptibility. The obtained values are in line with experimental data. This opens possibility to use such clusters to analyze the structural organization, vibrational and dielectric properties of the tellurium oxide glass.

Keywords: glasses, *ab initio* calculations, optical materials, nonlinear optics.

1. Introduction

The non-linear optics (NLO) deals with the physical phenomena related to the light-matter interaction in which the polarization versus field strength dependency is non-linear. The major problem of modern optoelectronics consists in searching new transparent materials with high optic non-linearity. Tellurite glasses are regarded as rather (if not the best) promising materials for NLO devices. Numerous experimental studies were devoted to investigating the NLO properties of the tellurite glasses in dependence on varying composition and synthesis treatment details and some useful relations have been reliably established [1] and references there.

Theoretical study of dielectric properties of glasses is hampered by the lack of credible structural models. There are two approaches to overcome this obstacle. One of them is based on assumption that the optical and electronic characteristics of glasses are similar to those of the crystalline lattices of the same chemical compositions. Unfortunately, only a restricted number of compositions may be found among known crystalline structures. An alternative approach, free of this shortcoming, deals with the molecular clusters of properly tailored chemical compositions.

The cluster approach consists in studying of quasi-molecular polyatomic systems mimicking the local structural units of a glass. Total geometry relaxation of such clusters gives a set of possible stable structural configurations. The crucial problem within such approach is a choice of initial geometry. The decision can be made based on chemical intuition or an analysis of the known crystalline structures. Anyway, such approach can give many stable configurations of the same chemical compositions. Relative energies of the structures allow an estimation of their abundance in the glassy specimens. Accordingly, studying dielectric properties of the most representative clusters, one can predict the properties of the glasses. The molecular clusters that preserve the chemical composition of the mimicked materials and do not content any additional atoms are referred as Bare Clusters (BC). BCs now show promise for being an effective tool in the characterization of the nanoparticles or the surfaces. Effectiveness of BC approach strongly depends on the number of atoms. The volume/surface ratio becomes the crucial factor when the

BC is used in studying bulky materials, because the chemical environment of the surface atoms is essentially disturbed due to breaking some of the chemical bonds. In order to sustain the adequate environment of the surface atoms with broken valence bonds, one can 'cap' the cluster with additional terminal groups. It is often accomplished with terminal H atoms, which are used to terminate the dangling bonds thus preserving electrical neutrality of clusters and valence saturation of atoms. Such approach is referred as H-capped (HC) clusters. It has an advantage of well mimicking the molecular structure inside a bulky material with sufficiently small clusters. At the same time, it suffers of shortcomings related to contributions of the artificial O-H bonds to the optic and dielectric properties of the clusters.

Both BC and HC approaches have been used in studying the tellurite glasses. The pioneering study dealt with very small BCs containing only one Te atom [2]. Starting from structural information borrowed from crystal chemistry of tellurites, the authors considered two basic units: the TeO_4 disphenoid and the TeO_3 pyramid. Both units were treated as anions $[TeO_4]^{4-}$ and $[TeO_3]^{2-}$ and were confronted with the analogous structural units in the α-TeO_2 and $ZnTeO_3$ crystals. It now appears that the idea to model the TeO_4 units of the electrically neutral TeO_2 framework by a heavily charged $[TeO_4]^{4-}$ anions is not a reasonable approach. However, despite of this inconsistence, the calculations yielded structural parameters in good agreement with experimental data. Besides, analysis of the calculated electronic structure revealed a rather high contribution of the 5s(Te) lone pairs to the HOMO states in both clusters.

An attempt to avoid the incorrectness related to overcharging of the TeO_4 cluster was performed in Ref [3]. Using the SCC-DV-$X\alpha$ method the authors studied the electronic structure of the TeO_4 cluster with net charge varying from 0 to -4e. It was found that the progressive electron charge transfer to TeO_4 causes the Te-O_{ax} bond weakening, thus leading to a reduction of the coordination number of a Te atom. Besides, it was shown that the excessive transferred charge is accumulated on the Te atom lone pair. The main shortcoming of the study was a neglect of the structural relaxation.

The most comprehensive and theoretically rigorous study of the tellurium oxide bare clusters was reported in Ref [4]. Geometry optimization for the $(TeO_2)_n$ (n=2 –6) cluster revealed a variety of stable configurations which included the Te atoms forming two, three, and four Te-O valence bonds. Analysis of the cohesive energy showed that the disphenoid-likeTeO_4 units are the most stable and the linkage of such units through corner sharing is preferred to edge sharing. It was also shown that, at increasing cluster dimension, the calculated energy of formation approaches the experimental cohesive energy of α-TeO_2 crystal. Confrontation of the simulated Raman spectra of the $(TeO_2)_n$ clusters with experimental data on glassy and crystalline tellurium oxide provided valuable information on the origin of certain spectral peaks [5]. All these findings confirmed suitability of the bare clusters for mimicking the local structural units of the TeO_2 glass. It seemed reasonable to use the clusters for revealing the origin of the huge non-linear susceptibility of the tellurite glasses.

This was done in Ref [6] in which bigger clusters (with n up to 12) of various structural organizations were considered. The calculated specific (per one TeO_2 formula unit) values of polarizability and the third-order hyperpolarizability slightly increase along with increasing n. Such increase was found the most prominent for the chain-like clusters. Moreover, it was shown that the $n \rightarrow \infty$ limit values well agree with the experimental data on linear and non-linear susceptibilities of the glassy TeO_2. This finding made it possible to associate the extremely high NLO properties of the TeO_2 glass with the presence of the long chain-like units with a highly delocalized electron states. In order to confirm this conclusion, the polarization properties of the long TeO_2-chains were analyzed with the use of the localized molecular orbital (LMO) approach [7]. Dipole moments, linear polarizabilities, and hyperpolarizabilities of the clusters were represented as sums of contributions of the individual chemical bonds and lone pairs. It was shown that the Te–O–Te bridges play a dominant role in the polarization properties of the long TeO_2-chains. This result directly indicated that the mechanism of the non-linear electronic polarization in the glassy tellurium oxide is mainly associated with the electron mobility within the chains

formed by polymerized Te–O–Te bridges. This favors the delocalization of the dielectric response (extended up to eighth-tenth neighbors from the point of a perturbation), thus enhancing the linear and high-order susceptibilities of this material.

However, almost all BCs $(TeO_2)_n$ have structural features which are very rare in the crystalline or glassy tellurium oxide. These are especially the double bridges Te<$^{O}_{O}$>Te and to a lesser extent the >Te=O groups with terminal Te=O bonds. The presence of such unusual structural units puts in doubt the transferability of the cluster properties to condensed TeO_2 materials. The appearance of such units is related to the valence unsaturation of the terminal O atoms. The HC clusters are free of such shortcoming.

The HC clusters are usually built on the ground of preliminary experimental information on the structure of tellurite crystals and glasses. The pioneering study deals with one TeO_4 unit and one TeO_3 unit linked by a Te-O-Te bridge [8]. A few years later, the same research group used a larger cluster having five TeO_4 units in a subsequent study [9]. H atoms terminated all dangling bonds in this cluster. Geometry optimization gave stable configurations with bond lengths that agree satisfactorily with experimental data obtained from diffraction experiments on tellurite glasses. Furthermore, such clusters were used for modelling the vibrational spectra of the tellurium oxide glasses. Calculated vibrational states of the TeO_4 and TeO_3 units linked by the Te-O-Te bridges made it possible to explain all prominent spectral features in Raman spectra of TeO_2 glass [8]. The success of the HC approach in the case of pure tellurium oxide stimulated similar studies of the mixed oxide systems. Clusters containing several TeO_4 and TeO_3 units linked to the WO_6 octahedron were used for modelling the structure of tungstate–tellurite glasses and provided a good description of the experimental data obtained by means of Raman spectroscopy [10]. Similar HC approaches were used in studying boro-tellurite [11], lead-vanadate-tellurate [12] and phospho-tellurite glasses [13].

HC clusters were also used for exploring the origin of the high non-linear polarizability of the tellurium oxides [14-15]. The small clusters consisting of one TeO_4 (TeO_3) unit capped by H

atoms were considered. Using the localized molecular orbital (LMO) approach, the static dipole moments, linear polarizabilities, and hyperpolarizabilities were represented as sums of contributions assigned to the individual chemical bonds and lone pairs. It was found that the TeO_4 structural unit exhibits much higher second hyperpolarizability than the TeO_3 structural unit, and that the Te atom lone pair gives the largest contribution which is very sensitive to the structural deformations. A similar approach was used in studying the modifier effect in the TeO_2-based glasses [16]. It was shown that the progressive substitution of the hydrogen atoms by alkali atoms in the $Te(OH)_3^+$ cluster increases both the linear polarizability and the second-order hyperpolarizability. This result, contradicting the experimental information, pointed out on the necessity to use larger clusters. Such clusters were used in *ab initio* study of linear and nonlinear optical properties of mixed tellurite–chalcogenide glasses [17]. The chain-like HC clusters of the TeX_2 (X=O, S, Se) composition were considered in that study. Geometry optimization showed that the inner part of the chains terminated by H atoms is more curved than that in the BCs considered by Soulis et al 2008 [7]. Despite this, the chain length effect (i.e. the increase of the specific values along with the elongation) was well confirmed for the linear and especially for non-linear polarizability. Besides, it was found that the chain length effect is more pronounced for heavier chalcogenides. Just recently, the TeO_2 nanoclusters have become the object of the intense experimental study and have shown many interesting properties [18]. In this regard, a theoretical study of HC clusters may shed a light on microscopic mechanisms of the hydroxylation process, as it was done for silica nanoclusters [19].

In the last decades, interest in cluster modelling has decreased. More attention was paid to computer modelling of infinite periodic systems. The efficiency of the standard DFT approaches (LDA and GGA) in reproducing the atomistic and electronic structure of paratellurite was first tested in 2004 [20]. It was found that the LDA method gives too dense and too hard α-TeO_2 crystal lattice. Contrariwise, the lattice is too large and too soft within the GGA approach. The bandgap value is too narrow in the GGA approach and slightly larger in LDA. However, both methods

provided this quantity smaller than the experimental estimation. Analysis of the charge density distribution argues a small covalent component to the bonding.

The structural and vibrational properties of all known TeO_2 polymorphs have been studied within LDA and GGA approaches in 2006 [21]. The same shortcomings of both approximations in reproducing the lattice volume were confirmed. In view of this, the experimental cell parameters were used in modeling of vibrational states. Such approach combined with the BLYP approximation provided a good agreement between calculated phonon frequencies and experiment. The same BLYP approximation was used later in the Molecular Dynamic modelling of the TeO_2 glass [22]. Inspection on the local structure of the glass phase reveals the presence of a great variety of TeO_n polyhedra with the predominance of TeO_4 units typical of the crystalline phases of TeO_2. Calculated IR and Raman spectra of amorphous TeO_2 are in good agreement with experimental data and provide an assignment of the most prominent experimental peaks to specific phonons.

Liu et al. [23] carried out a similar study on three TeO_2 polymorphs based on the PW91 approach. It was shown that the lone electron pairs have contributions near the Fermi energy level, and by forming a spatial cavity to store the *E*-pairs, the crystals are therefore microscopically labile, macroscopically compliant, and predisposed to polymorphism. In this study, much attention was paid to dielectric and optical properties of the materials. The dielectric function, reflectance and absorption coefficients in a wide energy range were analyzed.

Considerable effort has been devoted to explaining the high non-linearity of optical susceptibility of the tellurite materials. The first theoretical estimation of the third-order hyperpolarizability of paratellurite was reported in 2008 [24]. The $\chi^{(3)}$ values calculated for paratellurite with the use of B3LYP approximation were found to be of the same order as that measured for TeO_2 glass and much higher than the values computed for quartz which, in turn, were close to that of glassy silica. A similar approach was later used in studying other TeO_2 polymorphs [25].

The above review can be summarized as follows. Despite the widespread use of periodic ab initio calculations, the cluster approach remains a powerful technique providing new insight on many important issues such as structural units of the tellurite glasses, vibrational spectra interpretation, origin of the non-linear polarizability etc. Nevertheless, both cluster approaches, BC and HC, suffer from inherent shortcomings. The charged bulk clusters do not support the geometry optimization. Use of the neutral bulk clusters has a problem of dangling bonds that cause exaggerated valence binding activity or formation of the terminal Te=O bonds which were never observed experimentally. Application of the H-caped clusters necessitates using a priori structural model and inevitably involves the problem of extraction of the O-H bond contributions to energy and polarization. However, the acuteness of the problem of dangling bonds in BC approach and the problem of the O-H bond separation in HC approach decrease along with increase of the cluster dimension. As a supporting example we can refer to the study of a rather big cluster $(TeO_2)_{36}$ [26]. In this study, such cluster accurately cut off the paratellurite crystal lattice was used for calculating the third-order susceptibility. It was found that, in spite of many dangling bonds, the obtained theoretical estimations are in good agreement with the experimental data for paratellurite and glassy TeO_2. An additional advantage of the cluster approach compared to the periodic approach is possibility to use various interpretation schemes elaborated in quantum chemistry (such as MO population analysis and LMO representation) [7, 14].

The aim of this study is to investigate applicability of the HC approach to modelling the structure and properties of the tellurium oxide compounds. The paper is organized as follows. After describing the methods used, we present the results for three big HC clusters mimicking the structure of the TeO_2 compound. Finally, we compare the computational results with available experimental data and draw conclusions about the reliability of the cluster approach for studying the dielectric properties of the tellurium oxide.

2. Computational details

The calculations were performed within hybrid functional approximation to density functional theory (DFT) as implemented in Gaussian16 software packages [27]. The wave functions are expanded onto a set of localized atomic orbital (LCAO) basis set. The one parametric hybrid functional PBE0 [28] and the three parametric Becke, Lee-Yang-Parr (B3LYP) [29] methods were used to rule the mixing of exact Hartree-Fock (HF) exchange and DFT exchange. The exact exchange energy term (16.667%) was set in the instance of the PBE0 hybrid functional approach in accordance with previously published calculations [26] with results that very closely resembled experimental data for crystalline TeO_2.

The consistent Gaussian basis set of triple-zeta valence with polarization quality [30] for oxygen atoms was used in the calculations. Due to the complex electronic structure, pseudopotential method was applied to Te atoms with Gaussian double-valence basis set [31]. Kohn–Sham equations are solved iteratively to ensure the self-consistency within convergence criteria of 10^{-10} eV. The ground state structural parameters (lattice parameters and fractional positions of atoms) have been determined by the full geometry optimization. The structural relaxation was achieved with the convergence criterion for forces on atoms less than 0.003 eV/Å. The NLO properties of clusters were calculated by the finite difference method with respect to the electric field.

Calculations have shown that both B3LYP and PBE0 methods give very close results regarding structure and atomic vibrations, but differ in prediction of the polarization properties. Thus, discussing the structure, dynamics and energetics (up to the section IV.4) we use the B3LYP results. In the next sections, we compare the results of both methods.

3. Cluster modelling of TeO_2 oxide

3.1. Cluster I: $Te_{36}O_{99}H_{54} = 36TeO_2 + 27H_2O$

Initial cluster was built as a 3× 3×1 supercell of the α-TeO_2 crystal structure. It is shown in Fig. 1 (a, b). The cluster contains 36 disphenoid units (TeO_4) with 144 Te-O bonds. Structural parameters of paratellurite were borrowed from [32]. Half of the bonds are equatorial (1.878 Å

long), the other half is axial (2.122 Å long). Due to small cluster size, the majority of the Te atoms belong to the surface, i.e. have dangling Te-O bonds. Only 8 of 36 Te atoms have not dangling bonds. There are 8, 14 and 6 Te atoms with 1, 2 and 3 dangling Te-O bonds which are terminated by H atoms respectively. Thus, only 45 of 99 O atoms belong to the Te-O-Te bridges, other 54 are linked to the H atoms. Starting lengths of all O-H bonds were put equal to 0.96 Å and the Te-O-H angles equal to 109.5°.

Cluster structure optimized within the B3LYP approximation is shown in Fig. 1 (b, d). One can see that the optimized structure differs markedly from the initial configuration, i.e. from the regular framework of the corner-sharing TeO_4 disphenoids. If we assume that Te-O distances shorter than 2.3 Å correspond to valence bonds, then we find several unusual units (i.e. different from TeO_4 disphenoids and Te-O-Te bridges), namely 5 five-fold coordinated and 6 three-fold coordinated Te atoms and 2 three-fold coordinated O atoms in the optimized configuration. These transformations mainly occur through displacements of the terminal O-H groups. This leads to the formation of 4 Te-OH-Te bridges and to appearance strong intramolecular hydrogen O-H…O bonds with O…O distance shorter 2.6 Å. There are 8 such bonds in the optimized cluster configuration. Moreover, one quasi-isolated H_2O molecule weakly bound to the framework by the Te-O contact of 2.47 Å long appears.

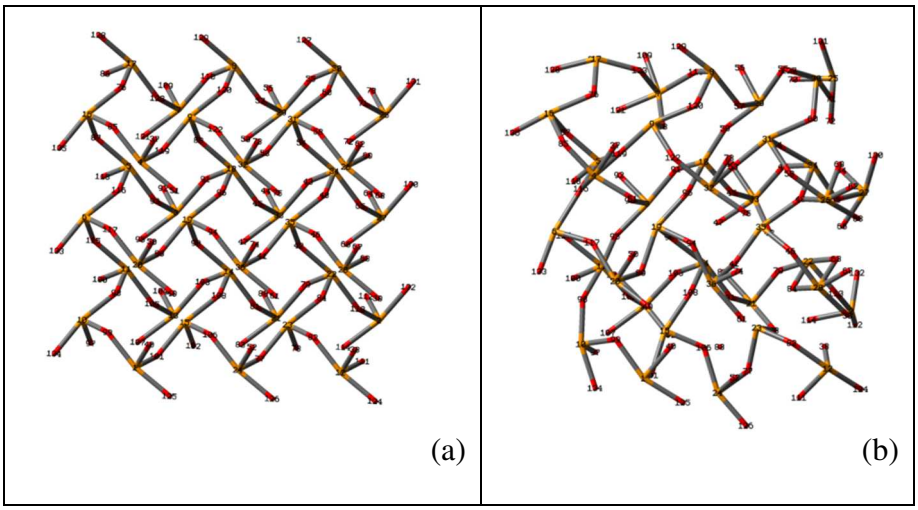

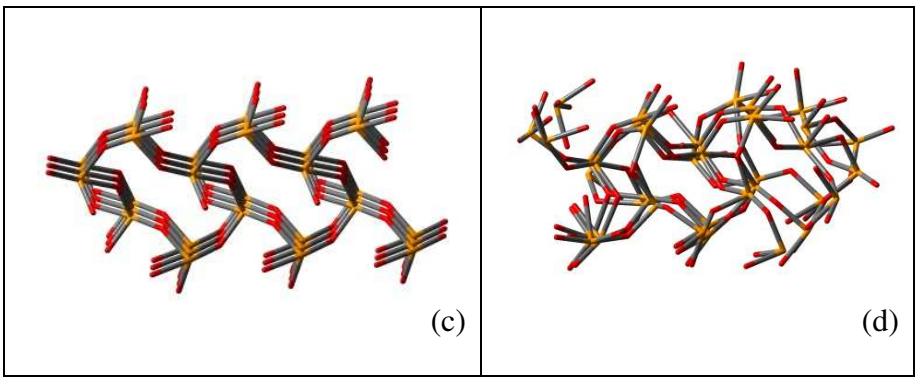

Fig. 1. Structure of cluster I in different projections before (a, c) and after (b, d) geometry optimization. Both structures are shown in xy (a, b) and xz (c, d) projections. The Te-O bonds are shown by tubes. The H atoms terminated dangling bonds are not shown.

3.2. Cluster II: $Te_{36}O_{96}H_{48} = 36TeO_2+24H_2O$

Initial cluster was built as a 2×2×2 supercell of the α-TeO_2 crystal structure. It is shown in Fig. 2 (a, b). The cluster contains 36 disphenoid units (TeO_4) with 144 Te-O bonds. Half of the bonds are equatorial (1.878 Å long), the other half is axial (2.122 Å long). Structural parameters of the initial configuration were determined by the preliminary DFT optimization of the paratellurite lattice [26]. They slightly differ from experimental values used in the preceding study

Only 8 of 36 Te atoms do not have any dangling bonds. There are 12, 12 and 4 Te atoms with 1, 2 and 3 dangling Te-O bonds which are terminated by H atoms respectively. Half of the 96 O atoms belong to the Te-O-Te bridges, the other half are linked to H atoms. Starting lengths of all O-H bonds were put equal to 0.98 Å and the Te-O-H angles within the interval 107°-119°.

Cluster structure optimized within the B3LYP approximation is shown in Fig. 2 (b,-d). One can see that the optimized structure differs markedly from the initial configuration, i.e. from the regular framework of the corner-sharing TeO_4 disphenoids. If we assume that Te-O distances shorter than 2.3 Å correspond to valence bonds, then we find several unusual units (i.e. different from TeO_4 disphenoids and Te-O-Te bridges), namely 8 five-fold coordinated and 6 three-fold coordinated Te atoms and 2 three-fold coordinated O atoms in the optimized configuration. These transformations mainly occur through displacements of the terminal O-H groups. This leads to the

formation of 2 Te-OH-Te bridges and to appearance of strong intramolecular hydrogen O-H…O bonds with O…O distance shorter 2.6 Å. There are 5 such bonds in the optimized cluster configuration. Moreover, the optimization leads to the appearance of 4 quasi-isolated H_2O molecules bound to the framework by the Te-O contacts of 2.3-2.5 Å long.

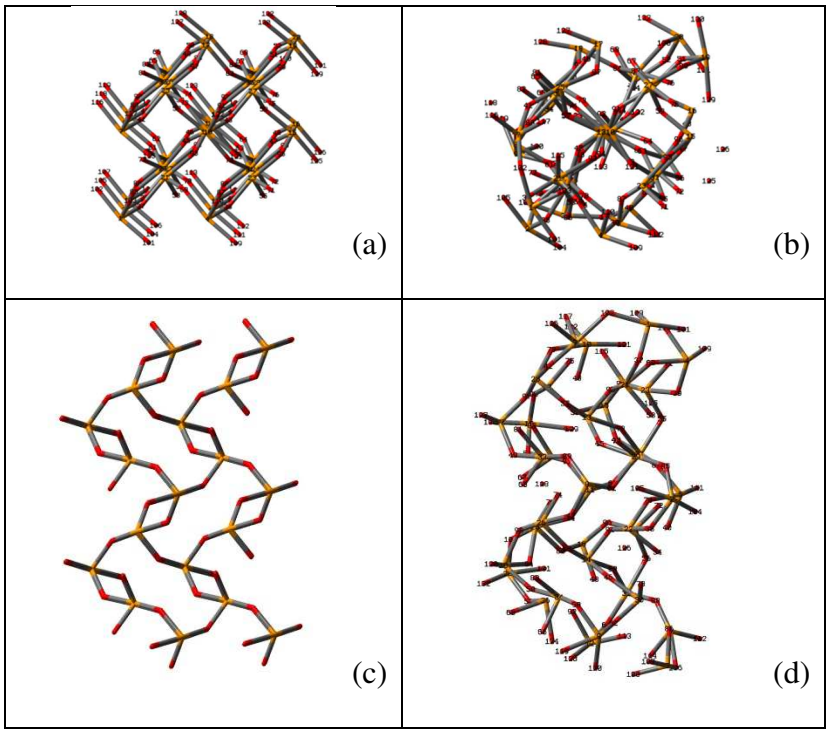

Fig. 2. Structure of cluster II in different projections before (a, c) and after (b, d) geometry optimization. Both structures are shown in *xy* (a, b) and *xz* (c, d) projections. The Te-O bonds are shown by tubes. The H atoms terminated dangling bonds are not shown.

3.3 Cluster III: $Te_{38}O_{97}H_{42} = 38TeO_2+21H_2O$

Initial cluster was built as a 3×3×1.5 supercell of the α-TeO_2 crystal structure. It is shown in Fig. 3 (a, b). Structural parameters of paratellurite were the same as in cluster I. Lengths of all dangling Te-O bonds were fixed at 2.03 Å. The cluster contains 38 disphenoid units (TeO4) with 152 Te-O bonds. Half of the bonds are equatorial (1.878 Å long), the other half is axial (2.122 Å long). Only 8 of 38 Te atoms have not dangling bonds. There are 18 and 12 Te atoms with 1 and 2 dangling bonds which are terminated by H atoms respectively. The 55 of 97 O atoms belong to

the Te-O-Te bridges, the others are linked to the H atoms. Starting lengths of all O-H bonds were put equal to 0.96 Å and the Te-O-H angles equal to 109.5°.

Cluster structure optimized within the B3LYP approximation is shown in Fig. 3 (b, d). One can see that the optimized structure differs markedly from the initial configuration, i.e. from the regular framework of the corner-sharing TeO_4 disphenoids. If we assume that Te-O distances shorter than 2.3 Å correspond to valence bonds, then we find several unusual units (i.e. different from TeO_4 disphenoids and Te-O-Te bridges), namely 12 five-fold coordinated and 2 three-fold coordinated Te atoms and 5 three-fold coordinated O atoms in the optimized configuration. These transformations mainly occur through displacements of the terminal O-H groups. This leads to the formation of 4 Te-OH-Te bridges and to appearance strong intramolecular hydrogen O-H…O bonds with O…O distances shorter than 2.6 Å. There are 10 such bonds in the optimized cluster configuration. Moreover, the optimization leads to the appearance of 2 quasi-isolated H_2O molecules bound to the framework by the Te-O contacts of about 2.4 Å long.

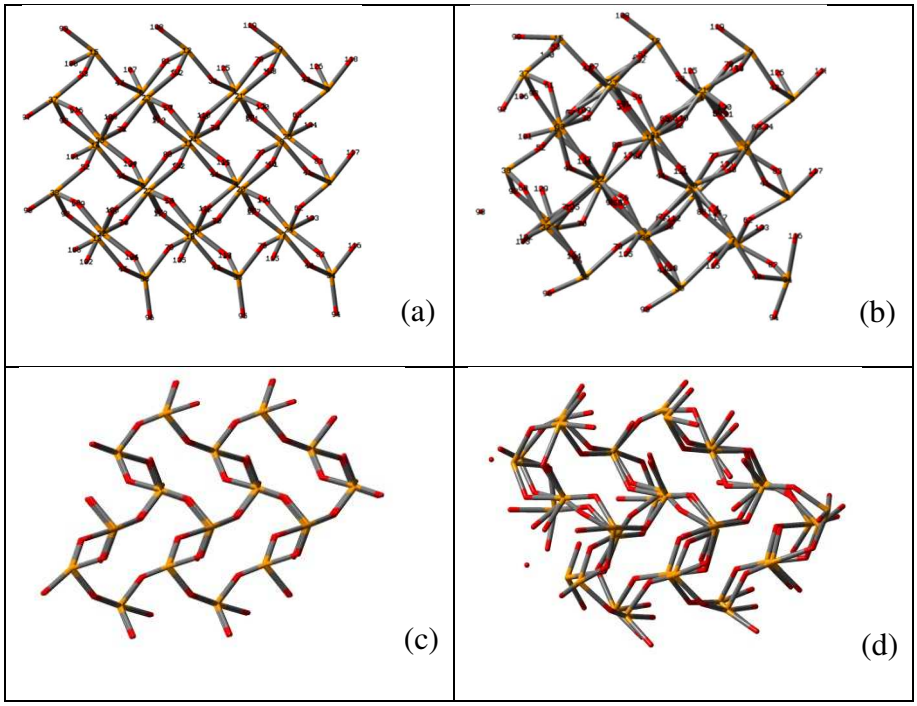

Fig. 3. Structure of cluster III in different projections before (a,c) and after (b,d) geometry optimization. The Te-O bonds are shown by tubes. The H atoms terminated dangling bonds are not shown.

4. Results and discussion

4.1. Structure

The above discussion shows that all studied structures are markedly distorted during optimization. In this section, we discuss the structural peculiarities. Recall that the TeO_4 units in the initial configurations of the three clusters were taken to be the same as in the paratellurite crystal structure. Thus, the length of half of the bonds was 1.878 Å and the one of the other half was 2.122 Å. These lengths are indicated in Fig. 4 by vertical dashed lines. The same figure shows that the Te-O bonds in optimized structures are longer, their lengths cover the wide interval up to 2.5 Å. Minimal bond lengthening occurs in the cluster III. The same cluster retains the difference between the lengths of axial and equatorial Te-O bonds, as evidenced by the presence of two almost equal-sized peaks on the distance distribution function. A detailed analysis shows that the optimization does not disturb the general structural constitution of the TeO_2 framework as a 3D net of corner sharing TeO_4 disphenoids. Despite significant distortion, the TeO_4 units retain a shape close to a disphenoid. This is confirmed by analysis of the O-Te-O valence angles. In almost all such units, there is one O-Te-O angle close to 160°. Another O-Te-O angle, situated in the almost perpendicular plane, is close to 90°.

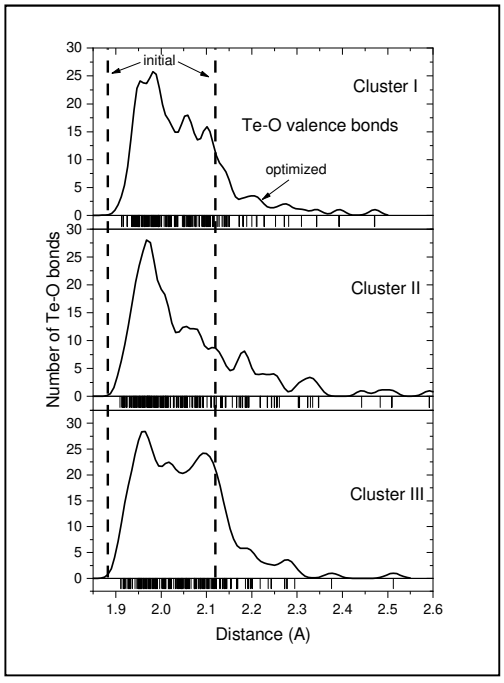

Fig. 4. Lengths of the Te-O bonds in three clusters (columns) and corresponding distance distribution functions (solid lines). Vertical dashed lines indicate initial bond lengths.

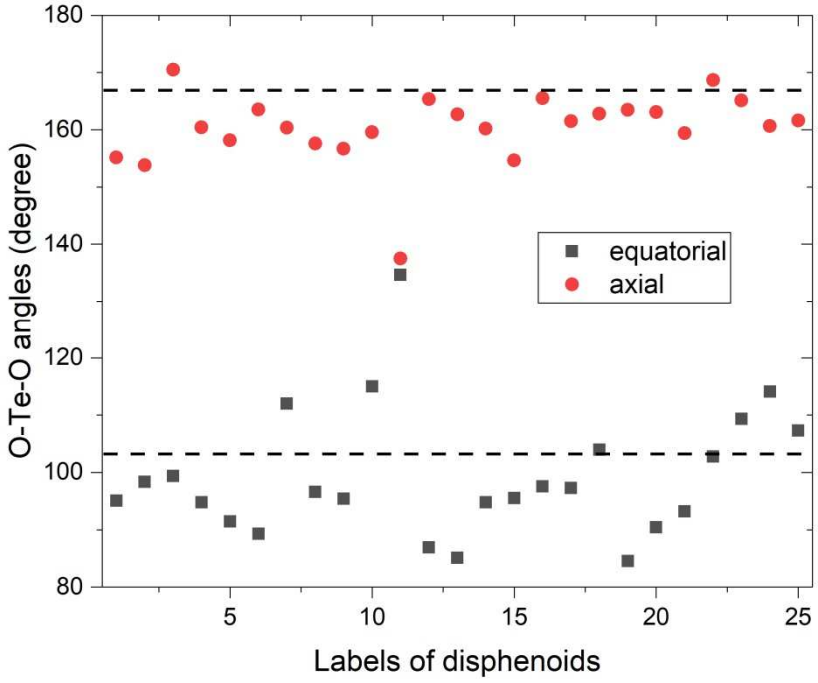

Fig 5. Valence angles between equatorial and axial Te-O bonds in the optimized structure of cluster III. Horizontal dashed lines indicate the angle values for the experimental paratellurite lattice.

Fig 5 shows such angles for the TeO_4 units in the cluster III. Recall that those angles are equal to 103° and 168° in the paratellurite lattice [32] and the angle distribution in glassy TeO_2 has two maxima at around 90° and 165° [22].

Another characteristic feature of the TeO_2 framework is the presence of Te-O-Te bridges with mean value close to 130° (this angle is equal to 139° in the paratellurite lattice). Fig. 6 shows the distribution of the bridges by the bridge angles for cluster I.

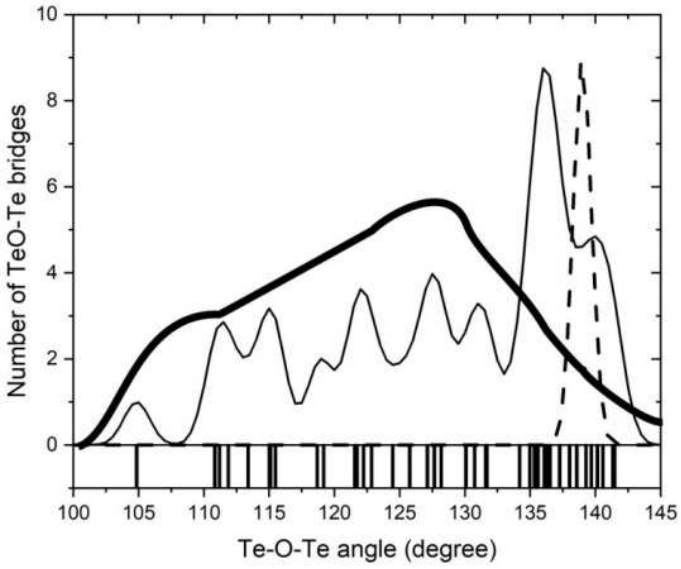

Fig. 6. Distribution of the Te-O-Te bridge angles in cluster I. The Molecular Dynamics data for TeO_2 glass [22] and the experimental data for paratellurite crystal [32] are shown be bold and dashed lines correspondingly

One can see that the distribution covers the interval between 100° and 145° with a high maximum at 138°. The position of the maximum is close to the Te-O-Te angle in the crystalline α-TeO_2 lattice (see dashed line in Fig. 6). The wide distribution of lower angle values resembles the angle distribution of the glassy TeO_2 (see bold line in Fig. 6). Thus, one can conclude that the structure of cluster I represents both crystalline and glassy states of TeO_2.

This suggestion is supported by analysis of the Pair Distribution Functions, which are shown in Figure 7. Indeed the PDFs calculated for the clusters under study are in line with the results obtained in Ref [22] for glassy TeO_2. At the same time, the PDF peak located at around 2 Å is doubly split and has two maxima at 1.95 Å and 2.15 Å. This fact points the difference between axial and equatorial bonds within the TeO_4 units, which is characteristic for the crystalline TeO_2.

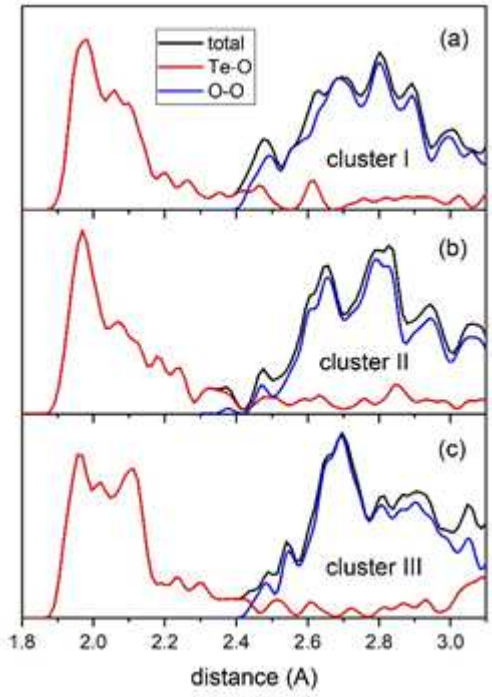

Fig 7. (a-c): calculated PDFs for the clusters under study

Let us try to summarize common features of the TeO_2 frameworks in the three optimized cluster structures. Upon optimization:

- ✓ length difference between axial and equatorial Te-O bond decreases but not disappears;
- ✓ the TeO_4 unit groups mainly keep the shape of a disphenoid;
- ✓ the Te-O-Te bridge angles and the PDF functions point to the coexistence of the structures typical for both crystalline and glassy states of TeO_2.

Now let us look at the local structural changes induced by adding terminal O-H bonds. Brief description of the optimized cluster structures in the preceding sections shows that the high mobility of the dangling bonds leads to the formation of new unusual structural units (let us call them 'defects'). Types and numbers of structural arrangements in the different clusters are listed in Table 1.

Table 1. Numbers of notable structural arrangements in the different clusters

Type of structural arrangements	Number of structural arrangements	Glass [22]

	Cluster I	Cluster II	Cluster III	
Te	36	36	38	
O_b	45	48	55	
Te-OH	54	48	42	
TeO_5	8 (22%)	8 (22%)	11 (29%)	8%
TeO_3	1 (3%)	5 (14%)	2 (5%)	20%
OTe_3	3	2	5	
Te-OH-Te	4	3	4	
H_2O…Te	1	3	2	
strong H-bonds	8	5	10	
Total	26	28	32	

One can see that the predominant defects are the TeO_5 units. They are formed in different ways. First way consists in the formation of the 3-fold coordinated O atoms (Fig 8a). Second way occurs through transformation of the dangling bonds in the bridge ones. This is accompanied by the formation of the Te-OH-Te bridges (Fig 8b). Another process, which involves three (or more) disphenoids, results in formation of TeO_5 units and TeO_3 units and one H_2O molecule (see Fig 8c). Besides, the TeO_3 units may appear due to the elongation of the Te-OH bonds, which is a consequence of the formation of the intra-molecular H-bonds (see Fig 8d).

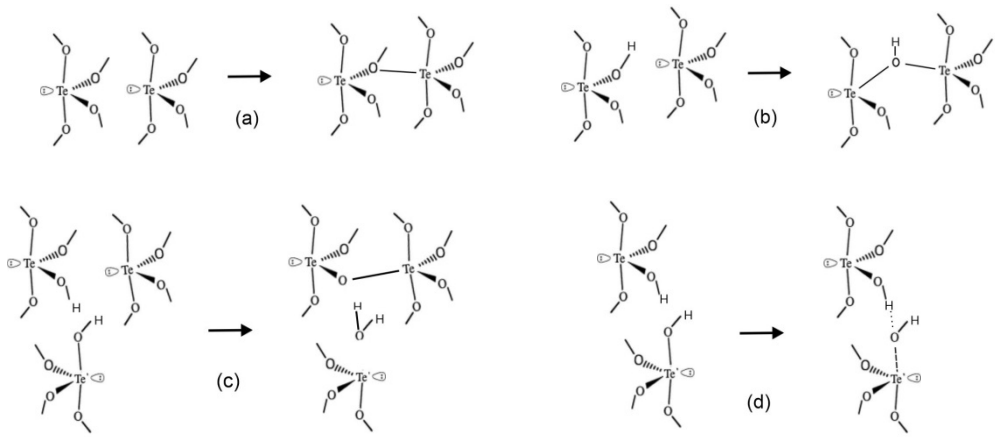

Fig 8. Schematic representation of the formation of some structural arrangements: TeO_5 + OTe_3 (a); TeO_5 + Te-OH-Te (b); TeO5 + TeO_3 + H_2O (c); $O_3TeO\ldots H$ (d).

Abundances of the TeO_5 and TeO_3 units in the glassy TeO_2 are about 8% and 20% correspondingly [22]. This differs from what follows from Table 1. The disagreement should be attributed to the effect of the terminal O-H bonds. Another consequence of this effect is the formation of quasi-free water molecules, more exactly the $Te\ldots O<^{H}_{H}$ units.

4.2. Energy

Compositions of all studied clusters can be represented as:

$$Te_nO_{2n+m}H_{2m} = n(TeO_2)+m(H_2O). \quad (1)$$

Corresponding n and m values are given in table 2, Such representation led us to the idea to test a similar decomposition for the total energy as:

$$E(\text{cluster}) \sim nE\left(TeO_2\right) + mE\left(H_2O\right) \quad (2)$$

The calculated total energies of the optimized structures are listed in Table 2. The same table shows the results of interpolating these values using Eq (2) with parameters $E(TeO_2)$ = 6735.64 a.u. and $E(H_2O)$ = 76.00 a.u.. One can see a very good agreement within an accuracy of ~10^{-5} % between calculated and estimated total energy.

Table 2. Total energies of the clusters (in a.u.) in comparison with estimations through Eq (2)

Cluster	Calculated	Estimated	*n*	*m*	$nE(TeO_2)$	$mE(H_2O)$
I	-244535.078021	-244535.04	36	27	242483.04	2052.00
II	-244307.052589	-244307.04	36	24	242483.04	1824.00
III	-257550.376037	-257550.32	38	21	255954.32	1596.00

This result is somewhat unexpected due to the variety of defects formed during the formation of clusters. Nevertheless, it opens up the possibility of using Eq (2) to estimate the energy of a cluster of arbitrary composition.

4.3. Vibrations

Frequencies of normal modes of the cluster cover a wide range from about 10 up to 3500 cm^{-1}. Phonon Densities of State (DOS) calculated for the three clusters are shown in Figure 9.

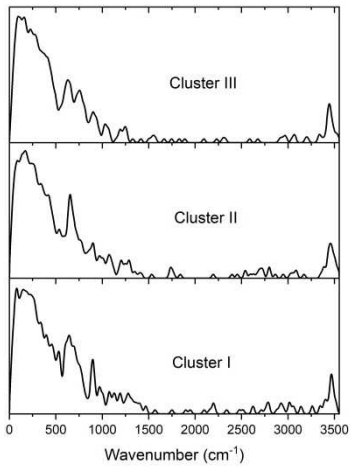

Fig. 9. Total phonon DOS for 3 clusters.

Analysis of the calculated eigenvectors allows suggesting the following approximate assignment shown in Table 3.

Table 3. Distribution of normal vibrations of clusters by types and frequency ranges

Type of vibrations		Number of modes		
	Frequency range	Cluster I	Cluster II	Cluster III
ν(O-H)	3300-3500	23	24	21
ν(O-H…O)	2200-3300	31	21	21
δ(H-O-H)	1700-1800	1	4	2
δ(Te-O-H) + rot(H_2O)	850-1500	82	59	51
ν_{as}(Te-O-Te) + τ(Te-OH)	700-850	28	31	39
ν(Te-OH) + τ(Te-OH)	500-700	83	79	69
ν_s(Te-O-Te) + τ(Te-OH)	400-500	49	34	46
ρ(Te-OH) + δ(O-Te-O)	120-400	190	182	181
Te atom oscillations	<120	74	100	95

Because we are interested in the properties of the TeO_2 framework, we should focus on the frequency range below 850 cm^{-1}. The reduced DOS of the clusters are shown in Fig. 10. The cluster's DOS mimics well the frequency distribution of the glassy TeO_2 calculated by the similar DFT method in Ref [22]. The best match is observed in DOS of cluster III. It is not trivial because of the significant mixing of vibrations of the TeO_2 framework with torsion oscillations of the terminal OH groups.

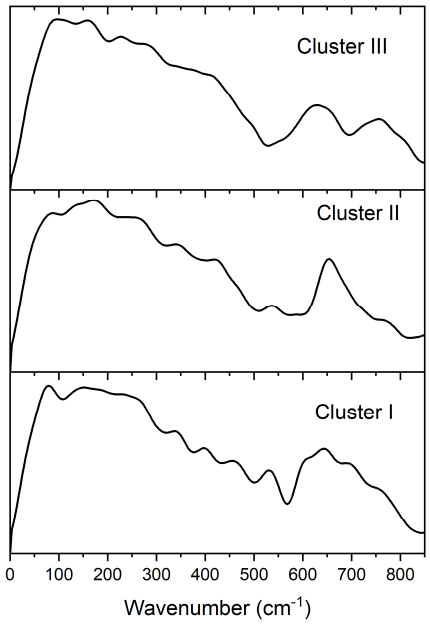

Fig. 10. Phonon DOS for the three clusters

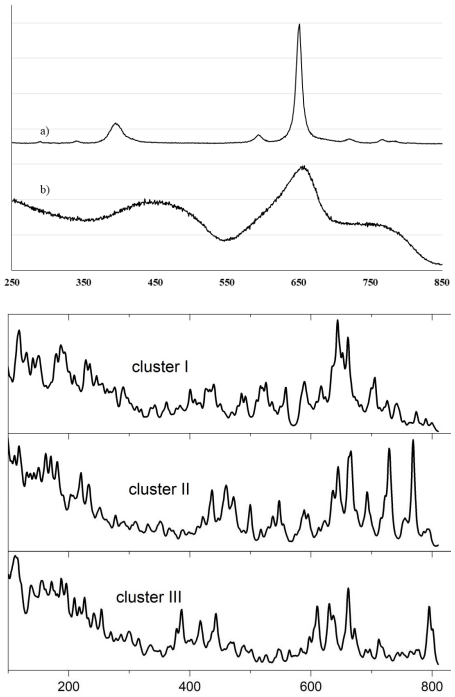

Fig. 11. Raman spectra of the three clusters and of TeO_2 glass (b) and of the paratellurite crystal (a)

Raman spectra of the clusters are presented in Fig 11. It is seen that they match with experimental spectra of the crystalline and glassy TeO_2. The best matching is inherent in the cluster III. Apparently, this is due to a lesser dangling bond content: proportions of dangling bonds in the initial configurations of clusters I, II and III are 37%, 33% and 28% respectively.

4.4 Electron bandgap

The bandgap values, estimated through the HOMO-LUMO differences for the three clusters, are close to each other. According to the B3LYP calculations, they are equal to 3.954, 3.586 and 3.647 eV for the clusters I, II and III correspondingly. According to the PBE0 calculations, are equal to 3.908, 3.561 and 3.711 eV for the clusters I, II and III respectively. It is noticeable that these values are in line with the experimental value $E_g = 3.75$ eV for the paratellurite [33].

4.5. Linear and non-linear polarizability and susceptibility

Since we are primarily interested in the modelling of the glassy material, we can omit discussing of the second-order hyperpolarizability. The calculated components of polarizability and third-order hyperpolarizability tensors are listed in Tables 4 and 5. For comparison with available experimental data, we use the orientation averaged values as:

$$\langle\alpha\rangle = \tfrac{1}{3}\left(\alpha_{xx} + \alpha_{yy} + \alpha_{zz}\right)$$

$$\langle\gamma\rangle = \tfrac{1}{5}\left(\gamma_{xxxx} + \gamma_{yyyy} + \gamma_{zzyy} + 2\gamma_{yyzz} + 2\gamma_{xxzz} + 2\gamma_{xxyy}\right)$$

and the values per one Te atom $\alpha_s = \langle\alpha\rangle / N$ and $\gamma_s = \langle\gamma\rangle / N$

Table 4. Calculated elements of polarizability tensor (in a.u.) and linear susceptibility (in SI units). Results obtained with B3LYP and PBE0 functionals are shown by direct and italic fonts respectively.

Cluster	TeO_2/H_2O	α_{xx}	α_{yy}	α_{zz}	$<\alpha>$	α_s	$\chi^{(1)}$(cryst)	$\chi^{(1)}$(glass)
I	36/27	1819	1327	1709	1618	44.9	4.47	3.66
		2040	*1486*	*1832*	*1786*	*49.6*	*4.93*	*4.04*
II	36/24	1998	1597	1365	1653	45.9	4.57	3.75
		2169	*1769*	*1524*	*1821*	*50.6*	*5.03*	*4.12*

III	38/21	1834	1687	1715	1746	45.9	4.57	3.75
		2029	*1882*	*1520*	*1810*	*47.6*	*4.74*	*3.89*
Suehara et al. [14]	1/2					60(40)		
Experimental							4.05 [34]	3.84 [35]

Table 5. Calculated elements of the third-order hyperpolarizability tensor (in 10^4 a.u.) and the non-linear susceptibility (in $\mathbf{10^{-22}\ m^2/V^2}$). Results obtained with B3LYP and PBE0 functionals are shown by direct and italic fonts respectively.

Cluster	γ_{xxxx}	γ_{yyyy}	γ_{zzzz}	γ_{yyzz}	γ_{xxzz}	γ_{xxyy}	$<\gamma>$	γ_s	$\chi^{(3)}$(cryst)	$\chi^{(3)}$(glass)
I	68.7	15.2	58.5	11.6	23.7	11.1	47.0	1.31	45.3	34.9
	93.9	*23.0*	*81.3*	*19.1*	*35.0*	*16.9*	*68.0*	*1.89*	*65.5*	*50.4*
II	119.8	53.4	17.2	7.8	12.8	29.2	58.0	1.61	55.9	43.0
	131.8	*70.1*	*27.8*	*9.9*	*16.8*	*36.6*	*71.3*	*1.98*	*68.6*	*52.8*
III	63.3	43.9	13.3	9.1	10.3	23.3	41.2	1.08	37.6	29.0
	79.4	*58.8*	*16.1*	*11.1*	*12.9*	*34.6*	*54.3*	*1.43*	*49.6*	*38.2*
experimental									**~100** [36]	

Using the calculated α_s and γ_s quantities one can estimate the linear $\chi^{(1)}$ and the third order non-linear $\chi^{(3)}$ susceptibilities following the methodology outlined in the Appendix. For transforming the computed microscopic quantities - polarizabilities and hyperpolarizabilities, into macroscopic characteristics - susceptibilities and hypersusceptibilities, we used two empiric parameters - experimental values of the mass densities *d* and the dielectric susceptibility $\chi^{(1)}$. They are different for the crystalline and glassy materials. In our estimations we used d=6.04 g/cm^3 [32] $\chi^{(1)}$=4.05 [34] for the crystalline α-TeO_2 and d=5.11 g/cm^3 [37] and $\chi^{(1)}$=3.84 [35] for glassy TeO_2. Using the above cited parameters one obtains the ratios:

$$\chi^{(1)}\text{(glass)}: \chi^{(1)}\text{(cryst)}=0.82 \text{ and } \chi^{(3)}\text{(glass)}: \chi^{(3)}\text{(cryst)}=0.77.$$

Estimations of all these quantities are listed in Tables 4-5.

One can see the theoretically estimated magnitudes of the $\chi^{(1)}$ for the crystalline TeO_2 are slightly overestimated compared to the experimental data. At the same time, similar estimation for the glassy TeO_2 agrees well with experiment. The theoretical estimations of $\chi^{(3)}$ are two-three times lesser than the experimental values. Similar underestimation of the $\chi^{(3)}$ were obtained in the theoretical study of the bare TeO_2 clusters [6, 15]. Our estimations predict that the $\chi^{(3)}$ of the glassy TeO_2 is by about 20% lower compared to the crystal.

Comparison of the B3LYP and PBE0 results shows that the former method gives larger values of both linear and non-linear susceptibilities. This can be considered as an advantage for the $\chi^{(3)}$ values and as a disadvantage for the $\chi^{(1)}$ values. In the whole, we can estimate availabilities of these two methods as quite comparable.

When comparing the results obtained for the three clusters, one can note a relatively large $\chi^{(1)}$ and $\chi^{(3)}$ values for cluster II. Analysis of individual tensor components shows that this is due to the enhanced polarizability (linear and elasticity and especially non-linear) of the cluster in x-direction. This is the vertical direction in Fig 2c. One can see that the cluster is maximally elongated in this direction. The chains of the Te-O-Te bridges along this direction consist of 8 links. Whereas the most long such chains in clusters I and III consist of only 6 and 5 links correspondingly (cf. Fig 1c and 3c). These results support the hypothesis of the chain length effect advanced in Refs [6, 7].

When using H-capped clusters, there is a difficulty associated with the need to exclude the contributions of the terminal hydroxyl groups. We cannot rigorously estimate these contributions to the $\chi^{(1)}$ and $\chi^{(3)}$ values. We can only appeal to the results of Ref [14], where such an assessment was made. It was shown in that study that the contributions of OH bonds reach 33% for $\chi^{(1)}$ and 20% for $\chi^{(3)}$. However, the TeO_2+2H_2O cluster studied in Ref [14] contained too many O-H bonds (as many as the Te-O bonds). This ratio is much lower for the clusters studied in this paper. This circumstance gives us reason to neglect these contributions.

In total, we can suggest that big HC clusters provide about the same $\chi^{(3)}$ values as BCs. Recall that sufficiently long chain-like $(TeO_2)_n$ (with n>6) provide a $\chi^{(3)}$ values comparable with experimental data [6, 7]. One can suggest that the bigger HC clusters also would give comparable $\chi^{(3)}$ values. Anyway, the presented results confirm that the enhanced NLO properties of TeO_2 are not determined by the local structural features.

5. Conclusions

Three tellurium oxide HC clusters have been studied within the B3LYP approximation of the DFT approach. Initial configurations of TeO_2 frameworks in the clusters were cut from the paratellurite crystal lattice. The clusters differ in the shape and size of the cut. Geometry optimization led to significant structural distortions, although it was shown that the TeO_4 units predominate in the optimized cluster structures. Besides, the unusual structural units, such as TeO_5, TeO_3 and OTe_3, appeared due to surface effects. All these defects were observed in the glassy tellurium oxide. At the same time, no defects atypical for the glass, such as terminal Te=O bonds or the Te<$^{O}_{O}$>Te double bridges, were found in the optimized structures of the HC clusters. This indicates the advantage of HC clusters compared to the bare $(TeO_2)_n$ clusters.

It was shown that the pair-distribution function and the distribution of the Te-O-Te bridge angles calculated for the optimized cluster structures match well with similar characteristics of glassy TeO_2. It was also shown that the TeO_4 units predominate in the optimized cluster structures. Basically, they keep the shape of disphenoids, which is confirmed by the analysis of Te-O bond lengths and O-Te-O valence angles. The combination of these facts points to the coexistence of the structures typical for both crystalline and glassy states of TeO_2, which determines the interest in the studied clusters as objects, with the help of which one can study the vitrification and the crystallization processes.

It was shown that the composition dependence of the calculated total energies of three clusters could be interpreted within the additivity approximation. This result allows us to estimate the energy value of an arbitrary cluster of composition $n(TeO_2)+m(H_2O)$.

The simulation of the vibrational states in the cluster under study shows the absence of imaginary frequency thus confirming their structural stability. It was shown that the calculated vibrational DOS function mimics well the frequency distribution of the glassy TeO_2, and the simulated Raman spectra of the clusters contain all prominent features characteristic for experimental spectra of both crystalline and glassy TeO_2. Analysis of the calculated eigenvectors allows suggesting an assignment for the characteristic vibrational states in a wide frequency interval.

The bandgap values, estimated through the HOMO-LUMO differences for the clusters under study, are close to the value derived experimentally for the paratellurite crystal. The calculated polarizability and the third-order hyperpolarizability coefficients were confronted with the experimental data for glassy and crystalline TeO_2. It is shown that the orientation average polarizability of the clusters agree well with the linear dielectric susceptibility of the tellurium oxide. At the same time, the calculated values of the average third-order hyperpolarizability of the clusters turned out to be 2-3 times lesser the experimental estimation. Thus, the origin of the high $\chi^{(3)}$ value of tellurium oxide still remains an open issue.

The obtained results confirmed the usefulness of the HC clusters or studying the structural organization, vibrational and dielectric properties of the tellurium oxide materials. The presence of many dangling Te-O bonds terminated by H atoms causes the optimized cluster structures to become noticeably different from a piece of the regular TeO_2 lattice. During the optimization the TeO_5, TeO_3, OTe_3 and Te-OH-Te units appear. Besides, some Te-O-H bridges approach each other and form strong O-H…O hydrogen bonds. Moreover, some Te-O and O-H bonds are broken and H_2O molecules appear. The results obtained using the HC approach have shown that the optimized cluster structure is far from the regular TeO_2 framework and successfully shifted to the structure of glassy TeO_2 composed by known structural units of amorphous material. At the same time the extra O-H bonds have a little effect on the electronic and optical properties.

The paper discusses various processes accompanying formation of the structural defects induced by the terminal O-H bonds. The results may provide a microscopic insight into hydroxylation of the tellurium oxide nanoclusters.

Acknowledgments

This work is supported by institutional grants from the French National Research Agency under the Investments for the future program with the reference ANR-10-LABX-0074-01 Sigma-LIM

References

1. R.F. Souza, M. Alencar, J. Hickmann, R. Kobayashi, L. Kassab, Appl. Phys. Lett. 89, (2006) 171917
2. A. Berthereau, E. Fargin, A. Villezusanna, R. Olazcuaga, G. Le Flem, L. Ducasse J. Sol. State Chem. 126 (1996) 143.
3. S. Suehara, S. Hishita, S. Inoue, A. Nukui, Phys. Rev. B 58 (1998) 14124
4. O. Noguera, M. Smirnov, P. Mirgorodsky, T. Merle-Méjean, P. Thomas, J.-C. Champarnaud-Mesjard, Phys. Rev. B 68 (2003) 094203
5. O. Noguera, M. Smirnov, A.P. Mirgorodsky, T. Merle-Méjean, P. Thomas, J.-C. Champarnaud-Mesjard, J. Non-Cryst Solids 345&346 (2004) 734
6. A.P. Mirgorodsky, M. Soulis, P. Thomas, T. Merle-Méjean, M. Smirnov, Phys. Rev. B 73 (2006) 134206
7. M. Soulis, T. Merle-Méjean, A.P. Mirgorodsky, O. Masson, E. Ohran, P. Thomas, M. Smirnov, J Non-Cryst Solids 354 (2008) 199
8. T. Uchino, T. Yoko, J. Non-Cryst. Solids 204 (1996) 243
9. H. Niida, T. Uchino, J. Jin, S.-H. Kim, T. Fukunaga, T. Yoko, J. Chem. Phys., 114 (2001) 459
10. V.O. Sokolov, V.G. Plotnichenko, V.V. Koltashev, E.M. Dianov, J. Non-Cryst. Solids 352 (2006) 5618
11. S. Rada, M. Culea, E. Culea, J. Non-Cryst Solids 354 (2008) 5491
12. S. Rada, M. Neumann, E. Culea, Solid State Ionics 181 (2010) 1164
13. T.Suzuki, T.W. Shiosaka, S. Miyoshi, Y. Ohishi, J. Non-Cryst. Solids 357 (2011) 2702
14. S. Suehara, P. Thomas, A.P. Mirgorodsky, T. Merle-Méjean, J.C. Champarnaud-Mesjard, T. Aizawa, S. Hishita, S. Todoroki, T. Konishi, S. Inoue, Phys. Rev. B 70 (2004) 205121
15. S. Suehara, T. Konishi, S. Inoue, Phys Rev.B 73 (2006) 092203
16. O. Noguera, S. Suehara. J. Non-Cryst. Solids 354 (2008) 188

17. Z Jin, I. Biaggio, J. Toulouse, J. Phys.: Condens. Matter 22 (2010) 65903
18. A. Amari, M.K. Al Mesfer, N.S. Alsaiari, M. Danish, A.M. Alshahrani, M.A. Tahoon, F.B. Rebah, Int. J. Electrochem. Sci. 16 (2021) 210235
19. A.M. Escatllar, P. Ugliengo, S.T. Bromley, Inorganics 5 (2017) 41
20. B.R. Sahu, L. Kleinman, Phys Rev B 69 (2004) 193101
21. M. Ceriotti, F. Pietrucci, M. Bernasconi, Phys Rev B 73 (2006) 104304
22. F. Pietrucci, S. Caravati, M. Bernasconi, Phys Rev B78 (2008) 064203
23. Y. Li, W. Fan, H. Sun, X. Cheng, P. Li, X. Zhao, J. Appl. Phys 107 (2010) 093506
24. M.B. Yahia, E. Orhan, A. Beltran, O. Masson, T. Merle-Méjean, A. Mirgorodski, P. Thomas, J Phys Chem B 112 (2008) 10777
25. N. Berkaine, E; Orhan, O. Masson, P. Thomas, J. Junquera, Phys Rev B 83 (2011) 245205
26. E M Roginskii, M.B. Smirnov, O. Noguera, O. Masson, P. Thomas, J. Phys.: Conf. Ser. 1461 (2020) 012137
27. M.J. Frisch, G.W. Trucks, H.B. Schlegel, G.E. Scuseria, M.A. Robb, J.R. Cheeseman, G. Scalmani, V. Barone, G.A. Petersson, H. Nakatsuji, X. Li, M. Caricato, A.V. Marenich, J. Bloino, B.G. Janesko, R. Gomperts, B. Mennucci, H.P. Hratchian, J.V. Ortiz, A.F. Izmaylov, J.L. Sonnenberg, D. Williams-Young, F. Ding, F. Lipparini, F. Egidi, J. Goings, B. Peng, A. Petrone, T. Henderson, D. Ranasinghe, V.G. Zakrzewski, J. Gao, N. Rega, G. Zheng, W. Liang, M. Hada, M. Ehara, K. Toyota, R. Fukuda, J. Hasegawa, M. Ishida, T. Nakajima, Y. Honda, O. Kitao, H. Nakai, T. Vreven, K. Throssell, J.A. Montgomery Jr, J.E. Peralta, F. Ogliaro, M.J. Bearpark, J.J. Heyd, E.N. Brothers, K.N. Kudin, V.N. Staroverov, T.A. Keith, R. Kobayashi, J. Normand, K. Raghavachari, A.P. Rendell, J.C. Burant, S.S. Iyengar, J. Tomasi, M. Cossi, J.M. Millam, M. Klene, C. Adamo, R. Cammi, J.W. Ochterski, R.L. Martin, K. Morokuma, O. Farkas, J.B. Foresman, D.J. Fox, Gaussian 16 Revision B.01 Gaussian Inc. Wallingford CT, 2016
28. C. Adamo, V. Barone, J. Chem. Phys. 110 (1999) 6158

29. A. D. Becke, J. Chem. Phys. 98 (1993) 5648

30. M.F. Peintinger, D.V. Oliveira, T. Bredow, J. Comput. Chem. 34 (2013) 451

31. J. Laun, D.V. Oliveira, T. Bredow, J. Comput. Chem. 39 (2018) 1285

32. P A Thomas, J. Phys. C 21 (1988) 4611

33. H. Jain, A.S. Nowick, Phys. Status Solidi A 67 (1981) 701

34. M. Okada, K. Takizawa, S. Ieiri, J. Appl. Phys. 48 (1977) 4163

35. R. A. H. El-Mallawany, J. Appl. Phys. 72 (1992) 1774

36. J.-R. Duclere, T. Hayakawa, E.M. Roginskii, M.B. Smirnov, A. Mirgorodsky, V. Couderc, O. Masson, M. Colas, O. Noguera, V. Rodrihuez, P. Thomas, J. Appl. Phys.123 (2018) 183105

37. R. A. H. El-Mallawany, Tellurite Glass Handbook, London, CRC Press, 2002

Appendix. Susceptibility and hypersusceptibility unit transformation

Dependence of the molecular dipole moment μ on the electric field *E* is decomposed in power series

$$\mu = \alpha E + \frac{1}{2}\beta E^3 + \frac{1}{6}\gamma E^3 ... \tag{A.1}$$

here α is polarizability, β and γ are hyperpolarizabilities.

Within the cluster approach, it is suggested that the studied molecule is a structural unit of the bulk material. Thus, the polarization *P* of such material is assumed equal to

$$P = \mu N \tag{A.2}$$

here *N* is the number of such units in the unit volume which can be estimated as

$$N = d / M \tag{A.3}$$

here *M* is mass of the cluster and *d* is the mass density of the modelled material. Dependence of the polarization *P* on the electric field E_0 is decomposed in power series as

$$P = \chi^{(1)} E_0 + \chi^{(2)} E_0^2 + \chi^{(3)} E_0^3 .... \tag{A.4}$$

in atomic units and as

$$P = \varepsilon_0 \left(\chi^{(1)} E_0 + \chi^{(2)} E_0^2 + \chi^{(3)} E_0^3 ... \right) \tag{A.5}$$

in SI units. Besides, one should keep in mind that the susceptibility and hypersusceptibility values $\chi^{(n)}$ in the two unit systems are related as

$$\chi^{(n)}(\text{SI}) = 4\pi\chi^{(n)}(\text{a.u.}) \tag{A.6}$$

In order to confront Eq. (A.1) with Eqs. (A.4-5) one must take into account the difference between the external field E_0 and the internal field E, which are related by the Lorentz factor

$$f_L = 1 + \frac{1}{3}\chi^{(1)}(\text{SI}) \tag{A.7}$$

as

$$E = f_L E_0 . \tag{A.8}$$

Using the relations (A.1-8) one can deduces

$$\chi^{(1)}(\text{a.u.}) = \alpha N f_L \ , \quad \chi^{(3)}(\text{a.u.}) = \frac{\gamma}{6} N f_L^3 \tag{A.9}$$

Transformation of $\chi^{(1)}$ into SI units is ruled by Eq.(A.6). Transformation of $\chi^{(3)}$ into SI units is performed as follows

$$\chi^{(3)}(\text{SI}) = 4\pi\chi^{(3)}(\text{a.u.})\left(\frac{E(\text{a.u.})}{E(\text{SI})}\right)^2 \tag{A.10}$$

The electric field is given in *e*/bohr^2 in atomic units and in V/m in SI units. Using Eq. (A.10) one obtains the relation

$$\chi^{(3)}(\text{m}^2/\text{V}^2) = \chi^{(3)}(\text{a.u.}) \times 0.475610^{-22} \tag{A.11}$$